Plug-and-Play Measurement-Device-Independent Quantum Key Distribution

Yong-Su Kim,[1,*] Yujun Choi,[1,2] Osung Kwon,[1] Sang-Wook Han,[1,†] and Sung Moon[1]

[1] *Quantum Information Research Center, Korea Institute of Science and Technology (KIST), Seoul, 136-791, Korea*
[2] *Department of Physics, Yonsei University, Seoul, 120-749, Korea*

(Dated: July 30, 2022)

Quantum key distribution (QKD) gaurantees unconditional communication security based on the laws of quantum physics. However, practical QKD suffers from a number of quantum hackings due to the device imperfections. From the security standpoint, measurement-device-independent quantum key distribution (MDI-QKD) is in the limelight since it eliminates all the possible loopholes in detection. Due to active control units for mode matching between the photons from remote parties, however, the implementation of MDI-QKD is highly impractical. In this article, we propose a novel method in which the indistinguishability issue is resolved without any active control unit. By introducing Plug-and-Play (P&P) concept into MDI-QKD, the indistinguishability between photons can naturally be guaranteed. We show the feasibility of P&P MDI-QKD with a proof-of-principle experiment.

arXiv:1501.03344v1 [quant-ph] 14 Jan 2015

INTRODUCTION

Quantum key distribution (QKD) has been focuses as the most feasible technology in quantum information science since the first QKD protocol (BB84 protocol) was introduced [1]. QKD allows two remote parties (Alice and Bob) to generate secret keys with the unconditional security by the laws of quantum physics. On the foundation of the immaculate theory, QKD has been developed in practical way and even made into full-packaged system [2]. However, doubts on the unconditional security of a QKD system have been continually raised. These doubts originate from gaps between ideal models and devices of the QKD system. For example, an ideal QKD protocol requires ideal single-photon source and detectors, however, implementating them is impossible with the current state of technology. These imperfections can be maliciously exploited, and make the QKD system vulnerable to various quantum hackings [3–12]. In order to overcome such weakness, device independent quantum key distribution (DI-QKD) was proposed [13, 14]. The security of DI-QKD does not depend on the devices' characteristics of the QKD system and thus guarantees unconditional security. However, DI-QKD is yet unrealizable because it requires loophole-free Bell test that has never been implemented.

The recently proposed measurement-device-independent quantum key distribution (MDI-QKD) closes the practicality gap of DI-QKD while compromising some aspects of security [15]. MDI-QKD closes all the possible loopholes in detection. Because detectors have been main targets of many quantum hacking attempts of the QKD system, MDI-QKD achieves immense improvement with respect to QKD system security. Furthermore, MDI-QKD can extend the maximum communication distance twice as much as that of ordinary QKD scheme. Owing to these outstanding aspects, MDI-QKD has been drawing much attention from the QKD community [16].

In the MDI-QKD protocol, Alice and Bob prepare singe-photon states independently, and send those to a third party (Charlie). The bit information is randomly encoded in one of the four states in the BB84 protocol. Then, Charlie performs Bell state measurements onto the incoming photons and publicly announces the measurement results to Alice and Bob. Finally, Alice and Bob can share secret keys after classical post-processing. The security of MDI-QKD is based on the time-reversed entanglement-based QKD protocol [17, 18], and thus, even if Eve possesses Charlie, she cannot obtain any information about the secret keys.

There have been some experimental implementations of MDI-QKD both in laboratories [19–21] and on deployed fiber networks [22, 23]. In order to successfully demonstrate MDI-QKD, the most critical issue in common is indistinguishability in spectral, polarization and temporal modes between the photons sent by Alice and Bob. Since the photons are prepared independently, it is difficult to make them identical. All the existing MDI-QKD experiments utilized active control units to match the modes. For instance, to match the spectrum, frequency locked lasers with gas cells or distributed feedback lasers with temperature controllers were used. However, the use of the active control units is not only a nuisance for practical implementation, but also an obstacle for commercialization due to their exorbitant costs and system complexity. For the practical MDI-QKD implementation, therefore, it is necessary to solve the indistinguishability issue with a more convenient and inexpensive method.

In this article, we propose a new scheme of MDI-QKD, named Plug-and-Play MDI-QKD (P&P MDI-

* yong-su.kim@kist.re.kr
† swhan@kist.re.kr

QKD), that minimize the use of active control units. We introduce how one can bring the Plug-and-Play architecture into MDI-QKD. Then, we will show the proof-of-principle experiment on P&P MDI-QKD that shows the practicality of the new scheme.

RESULTS

Plug-and-Play MDI-QKD

Figure 1(a) shows the a schematic of conventional MDI-QKD protocol with weak coherent pulses (WCP). An encoder randomly assigns one of the four BB84 states to the pulse. The four BB84 states can be either in the Z-basis ($|0\rangle$ and $|1\rangle$) or the X-basis ($|\pm\rangle = \frac{1}{\sqrt{2}}(|0\rangle \pm |1\rangle)$. An intensity modulator (IM) generates decoy states of the pulses to protect the protocol from the photon number splitting attack [25, 26]. Alice and Bob transmit the pulses to Charlie, and then he performs the Bell state measurements (BSM). Note that one can implement a BSM that can distinguish two Bell states, $|\psi^+\rangle$ and $|\psi^-\rangle$, with only linear optics and two-photon interference. This incomplete BSM is enough for implementing MDI-QKD. After performing the BSM, Charlie announces the results publicly, and then Alice and Bob can generate sifted keys only when their bases are identical [15].

It is interesting to note that there is and unavoidable error rate of 25% in X-basis caused by the pulses containing multi-photons of the coherent pulses. Thus, with the WCP implementation, Alice and Bob generate secret keys only using the Z-basis, and the X-basis is used to monitor Eve's attack. If one implements MDI-QKD with single-photon states, both the Z- and X-bases can be used for generating secret keys.

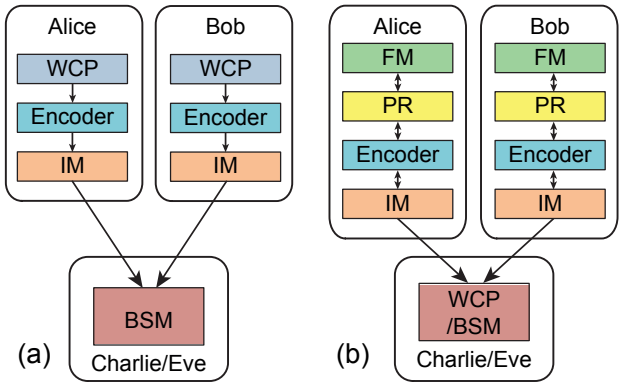

FIG. 1: Schematic diagrams of (a) conventional MDI-QKD protocol and (b) Plug-and-Play MDI-QKD protocol. WCP : weak coherent pulse, Encoder : the device that encodes bit information, IM : intensity modulator, FM : faraday mirror, PR : phase randomizer, BSM : Bell state measurement. In a conventional MDI-QKD protocol, Alice and Bob prepare pulses independently, and send them to Charlie for Bell state measurement. In Plug-and-Play MDI-QKD, Charlie initially launches pulses to Alice and Bob, and then Alice and Bob reflect back the pulses to Charlie.

In the P&P MDI-QKD protocol shown in Fig. 1(b), the entire process is similar, but slightly different from that of the conventional MDI-QKD protocol. First, Charlie sends WCPs to Alice and Bob through a 50:50 beamsplitter (not shown in Fig. 1(b)). The pulse is transmitted through an optical fiber, and then reflected by a Faraday mirror (FM) of Alice (Bob). A phase randomizer (PR) randomizes the phase of the reflected pulse in order to prevent single-photon interference [27, 28]. The encoder and the IM randomly assign a bit and decoy states to the pulse. Then, the pulse is retransmitted through the same optical fiber from Alice (Bob) to Charlie. After that, BSM and post-processing are followed to obtain secret keys.

The P&P MDI-QKD has remarkable features in the mode matching issue. Starting from the same laser source, the spectral modes of the pulses sent by Charlie are already identical. Moreover, the polarization mode dispersion during the optical fiber transmission can be automatically compensated due to the Plug-and-Play architecture [24]. With these aspects, we can minimize efforts for mode matching with P&P MDI-QKD.

It is necessary to note how the plug-and-play architecture affects the security of MDI-QKD. Note that the original MDI-QKD provides unconditional security against any detector side channel attack. Since the plug-and-play architecture does not disturb the measurement setup of the MDI-QKD, the unconditional security against the detector side channel attacks can be also guaranteed. On the other hand, the plug-and-play architecture may weaken the security against the hackings on sources. These vulnerabilities, however, can easily be circumvented by applying simple techniques that are already developed for an ordinary P&P QKD [29].

Experimental setup

In order to see the feasibility of the proposed P&P MDI-QKD scheme, we perform a proof-of-principle experiment. Figure 2(a) represents an experimental concept for a bulk-optic implementation of the P&P MDI-QKD with polarization encoding. For the simplicity, we employ a continuous-wave laser diode (CW-LD). Note that even though there is an ambiguity in temporal overlap of photons, it is known that two-photon interference can be observed using a CW-LD that is essential for the MDI-QKD [28].

In Fig. 2(a), the laser beam emitted from the CW-LD is transmitted toward a beamsplitter (BS) through an

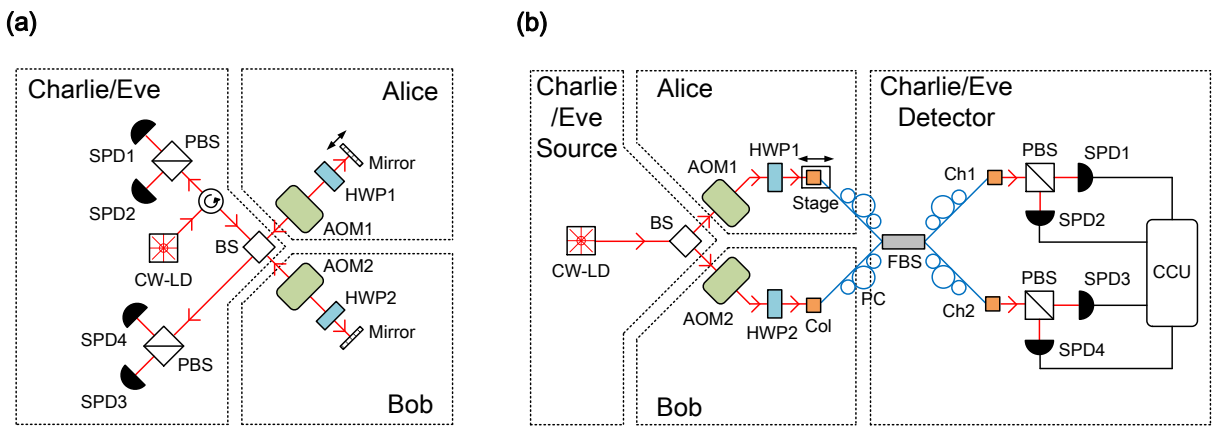

FIG. 2: (a) Experimental concept and (b) experimental setup of the proof-of-principle P&P MDI-QKD. CW-LD : continuous-wave laser diode, BS : beamsplitter, AOM : acousto-optic modulator, HWP : half waveplate, Col : collimation lens, Stage : translational stage, PC : polarization controller, FBS : fiber beamsplitter, Ch1,2 : Channel 1,2, PBS : polarizing beamsplitter, SPD : singe-photon detector, CCU : coincidence counting unit. Experimental concept is a physical implementation of P&P MDI-QKD in bulk optics. Experimental setup is an extension of the experimental concept for expedience. All the experiment is done with the experimental setup.

optical circulator indicated by a bending arrow mark in a circle. The beam is separated into two paths (Alice and Bob) by a beamsplitter (BS). The separated beams go into acousto-optic modulators (AOM) which modulate the beams independently. The AOMs randomize the phases of the diffracted beams, and thus suppress the single-photon interference [27, 28]. The first-order diffracted beams go through half waveplates that encode bits to the beams into the polarization modes. Note that, in the setup, the AOMs and the HWPs are substitutes for the PRs and the encoders in Fig. 1(b), respectively. After encoding, the beams are reflected by mirrors, and sent back to Charlie. One can scan the position of the Alice's mirror in order to match the temporal modes. Including the BS, the two polarizing beamsplitters (PBS) and the four singe-photon detectors (SPD) implement a BSM with polarization encoding. For BSM, $|\psi^+\rangle$ corresponds to the coincidence detection between SPD1 and SPD2 or between SPD3 and SPD4, and $|\psi^-\rangle$ corresponds to the coincidence detection between SPD1 and SPD4 or between SPD2 and SPD3 [15].

For the sake of convenience, we implement an experimental setup as shown in Fig. 2(b), which is a simple extension of the experimental concept of Fig. 2(a). Though the source and detector parts of Charlie are spatially separated, the setup is equivalent to the concept. All the procedures are the same except that a fiber beamsplitter (FBS) is used for the BSM which makes the optical alignment easier. In Fig. 2(b), after passing through the HWPs, the beams are interfere at the FBS. The optical path length can be adjusted by scanning Alice's collimating lens which is located before the FBS. Four polarization controllers (PC) are used to maintain the polarization mode in the fiber. The outputs of the FBS, Ch1 and Ch2, are transmitted to the PBS and the SPDs for BSM. A coincidence counting unit (CCU) records single counts of each SPD's output and coincidence counts between different SPD's outputs [30]. Detailed experimental setup can be found in the Method section.

Experiment result

Two-photon interference is essential for the proposed scheme as for the conventional MDI-QKD because it is a fundamental element of the BSM. To make the path lengths of Alice and Bob equal, we adjust Alice's optical path length by scanning the collimating lens.

Since we are interested in the BSM with two-photon interference, single-photon interference should be washed out. This can be done by inserting independently modulated AOMs in the whole interferometer arms [27, 28]. In order to measure the single-photon and two-photon interference, Ch1 and Ch2 were directly connected to two SPDs. When two AOMs are synchronized, one can see clear single-photon interference, see Fig. 3(a). As shown in Fig. 3(b), however, the single-photon interference is washed out when two AOMs are independently modulated.

After checking the independently modulated AOMs efficiently suppress the single-photon interference, we observed two-photon interference which is equivalent to the MDI-QKD protocol. Because of the long coherence length of CW-LD, it was difficult to observe Hong-Ou-Mandel (HOM) dip while scanning the optical path length. On behalf of that, two-photon interference was

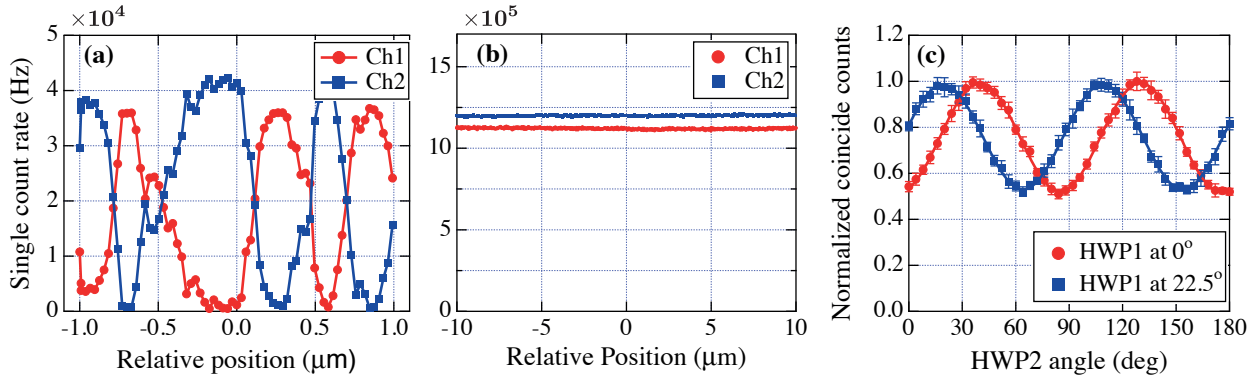

FIG. 3: Single-photon interference with (a) synchronized AOMs and (b) independently operating AOMs. The independently operating AOMs degrade single-photon interference. (c) Two-photon interference with independently operating AOMs. The two-photon interference is observed by rotating HWP2 by 4° while HWP1 is fixed at a certain angle. Solid curves and error bars denote fitted sine curves and standard deviations, respectively.

measured by changing one of the polarization states of two inputs, see Fig. 3(c). The error bars and solid lines are the experimental standard deviations and sine fittings, respectively. The interference visibilities are measured to be $31.3 \pm 0.89\%$ and $30.1 \pm 0.77\%$ when HWP1 was fixed at 0° and 22.5°, respectively. These visibilities correspond to $47.7 \pm 0.90\%$ and $46.3 \pm 0.78\%$ for the conventional HOM dip, and these are close to the classical limit of two-photon interference visibility, 50%.

Finally, we performed BSM and estimated expected quantum bit error rate (QBER) according to the MDI-QKD protocol.The BSM setup shown in Fig. 2(b) was restored for this purpose. The Bell state measurement result with average photon numbers for Alice and Bob of 0.5 is shown in Fig. 4. The horizontal axis represents the encoded polarization states by Alice and Bob. For example, HV is that Alice and Bob send horizontal and vertical polarization states, respectively. For each polarization states, the coincidence counts were accumulated for 10 minutes. From the data, we obtained average coincidence count rates and standard deviations, which are indicated by solid bars and error bars of Fig. 4, respectively. The QBERs for this case as well as $\mu = 0.3$ case are shown in Table I. Taking the theoretical QBERs, 0% for Z-basis and 25% for X-basis, into account, the QBERs are small enough to verify the feasibility of P&P MDI-QKD. The QBER estimation process is described in the Method section.

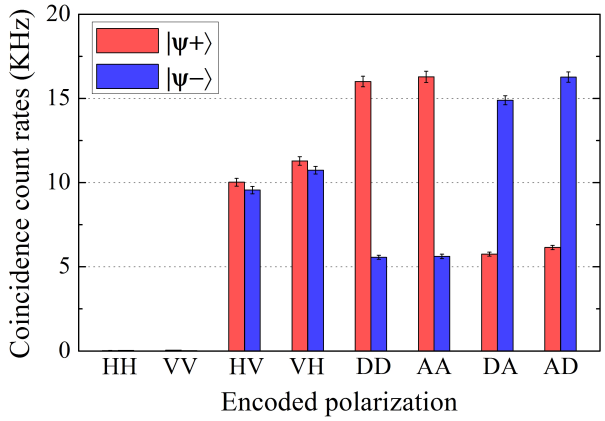

FIG. 4: Results of Bell state measurement when average photon number μ is (a) 0.3 and (b) 0.5. The average photon numbers of Alice and Bob are equal for each case. The horizontal axis denotes the polarization encoding by Alice and Bob, e.g., HV denote Alice and Bob send horizontal and vertical polarization, respectively. Solid bars and error bars denote average coincidence count rates and standard deviations, respectively.

DISCUSSION

The P&P MDI-QKD has several advantages in comparison to the conventional MDI-QKD. The most important advantage is that one can minimize the use of active control units. In time-bin phase encoding with pulsed laser source, for example, initial mode matching for spectrum is already done by utilizing the same laser.

TABLE I: QBERs of P&P MDI-QKD

Basis	QBER	
	μ=0.3	μ=0.5
Z	0.37±0.05%	0.30±0.03%
X	26.5±0.46%	26.7±0.35%

The phase reference of time-bins pulses sent by Alice and Bob are also automatically matched since Charlie can posses the interferometer. These advantages will be a great merit for the practicality. Moreover, the Plug-and-Play architecture guarantees the robustness against polarization change of fiber. This robustness will give superior performance in implementing the MDI-QKD on deployed optical fibers. Finally, P&P MDI-QKD is appropriate for realizing MDI-QKD network. Since Charlie (server) has a source and detectors, Alice and Bob (users) need only encoding devices. If the server is located at a base station or a satellite, users can communicate securely with inexpensive and compact size devices. In conclusion, P&P MDI-QKD will facilitate practical implementation of MDI-QKD, and will begin a new phase toward ultimate secure communication.

METHOD

Experimental setup

CW-LD is a 780nm single mode laser diode. Between CW-LD and the BS, a polarizer and neutral density filters were inserted (not shown in Fig. 2(b)). Two AOMs were controlled by two AOM drivers operating independently. The operating frequencies of AOM drivers were identical (40MHz) to minimize the frequency shift of the diffracted beams. By adjusting AOM drivers' power, the average photon numbers of Alice and Bob were set the same. Four SPDs are silicon avalanche photodiode, which has quantum efficiency of about 50% at 780nm. The CCU was implemented with an FPGA, and the coincidence window of CCU is about 8ns [30].

QBER analysis

In the Z-basis, the erroneous coincidence counts are both $|\psi^+\rangle$ and $|\psi^-\rangle$ for HH or VV. In the X-basis, erroneous coincidence counts are $|\psi^-\rangle$ for DD or AA and $|\psi^+\rangle$ for DA or AD. Based on that, we could calculate the QBER for each case. The QBERs are given by:

$$E_Z = \frac{C_{HH} + C_{VV}}{C_{HH} + C_{VV} + C_{HV} + C_{VH}} \tag{1}$$

$$E_X = \frac{C^+_{DD} + C^-_{AA} + C^+_{DA} + C^+_{AD}}{C_{DD} + C_{AA} + C_{DA} + C_{AD}} \tag{2}$$

where E_Z and E_X stands for the QBER of the Z- and X-basis, respectively, and

$$C_{ij} = C^+_{ij} + C^-_{ij} \tag{3}$$

where $C^{\pm}_{ij}$ is the coincidence count corresponding to $|\psi^{\pm}\rangle$, and the subscript ij is the encoding polarization by Alice and Bob, respectively.

ACKNOWLEDGEMENT

This work was supported in part by the IT R&D program of MSIP/KEIT[10044559], and the ICT R&D program of MSIP/IITP[2014-044-014-002].

[1] Bennett, C. H. & Brassard, G. Quantum cryptography: public key distribution and coin tossing. *Proceedings of the IEEE International Conference on Computers, Systems and Signal Processing*, Bangalore, India 175179 (1984).

[2] For example, http://idquantique.com/

[3] Makarov, V., Anisimov, A. & Skaar, J. Effects of detector efficiency mismatch on security of quantum cryptosystems. *Phys. Rev. A* **74**, 022313 (2006).

[4] Lamas-Linares, A. & Kurtsiefer, C. Breaking a quantum key distribution system through a timing side channel. *Opt. Express* **15**, 93889393 (2007).

[5] Lydersen, L. *et al.* Hacking commercial quantum cryptography systems by tailored bright illumination. *Nature Photon.* **4**, 686689 (2010).

[6] Weier, H. *et al.* Quantum eavesdropping without interception: an attack exploiting the dead time of single-photon detectors. *New J. Phys.* **13**, 073024 (2011).

[7] Jain, N. *et al.* Device calibration impacts security of quantum key distribution. *Phys. Rev. Lett.* **107**, 110501 (2011).

[8] Xu, F., Qi, B. & Lo, H.-K. Experimental demonstration of phase-remapping attack in a practical quantum key distribution system. *New J. Phys.* **12**, 113026 (2010).

[9] Sun, S.-H., Jiang, M.-S. & Liang, L.-M. Passive Faraday-mirror attack in a practical two-way quantum-key-distribution system. *Phys. Rev. A* **83**, 062331 (2011).

[10] Huang, J.-Z. *et al.* Quantum hacking on continuous-variable quantum key distribution system using a wavelength attack. *Phys. Rev. A* **87**, 062329 (2013).

[11] Tang, Y.-L. *et al.* Source attack of decoy-state quantum key distribution using phase information. *Phys. Rev. A* **88**, 022308 (2013).

[12] Jouguet, P., Kunz-Jacques, S. & Diamanti, E. Preventing calibration attacks on the local oscillator in continuous-variable quantum key distribution. *Phys. Rev. A* **87**, 062313 (2013).

[13] Mayers, D. & Yao, A. Quantum cryptography with imperfect apparatus. in *Proc. 39th Ann. Symp. Foundations Comp. Sci.* 503509 (IEEE, 1998).

[14] Acin, A. *et al.* Device-independent security of quantum cryptography against collective attacks. *Phys. Rev. Lett.* **98**, 230501 (2007).

[15] Lo, H.-K., Curty, M. & Qi, B. Measurement-device-independent quantum key distribution. *Phys. Rev. Lett.* **108**, 130503 (2012).

[16] Lo, H.-K., Curty, M. & Tamaki K. Secure quantum key distribution *Nature Photon.* **8**, 595 (2014).

[17] Biham, E., Huttner, B. & Mor, T. Quantum cryptographic network based on quantum memories. *Phys. Rev. A* **54**, 26512658 (1996).

[18] Inamori, H. Security of practical time-reversed EPR quantum key distribution. *Algorithmica* **34**, 340365 (2002).

[19] Ferreira da Silva, T. *et al.* Proof-of-principle demonstration of measurement-device-independent quantum key distribution using polarization qubits. *Phys. Rev. A* **88**, 052303 (2013).

[20] Liu, Y. *et al.* Experimental measurement-device-independent quantum key distribution. *Phys. Rev. Lett.* **111**, 130502 (2013).

[21] Tang, Z. *et al.* Experimental demonstration of polarization encoding measurement-device-independent quantum key distribution. *Phys. Rev. Lett.* **112**, 190503 (2014).

[22] Rubenok, A. *et al.* Real-world two-photon interference and proof-of-principle quantum key distribution immune to detector attacks. *Phys. Rev. Lett.* **111**, 130501 (2013).

[23] Tang, Y.-L. *et al.* Field test of measurement-device-independent quantum key distribution. Preprint at http://lanl.arXiv.org/abs/1408.2330 (2014).

[24] Muller, A. *et al.* Plug and play systems for quantum cryptography. *Appl. Phys. Lett.* **70**, 793-795 (1997).

[25] Hwang, W.-Y. Quantum key distribution with high loss: toward global secure communication. *Phys. Rev. Lett.* **91**, 057901 (2003).

[26] Lo, H.-K., Ma, X. & Chen, K. Decoy state quantum key distribution. *Phys. Rev. Lett.* **94**, 230504 (2005).

[27] Kim, Y.-S., Slattery, O., Kuo, P. S. & Tang, X. Conditions for two-photon interference with coherent pulses. *Phys. Rev. A* **87**, 063843 (2013).

[28] Kim, Y.-S., Slattery, O., Kuo, P. S. & Tang, X. Two-photon interference with continuous-wave multi-mode coherent light. *Opt. Express* **22**, 36113620 (2014).

[29] Gisin, N. *et al.* Trojan-horse attacks on quantum-key-distribution systems. *Phys. Rev. A* **73**, 022320 (2006).

[30] Park, B.-K. *et al.* A high-performance reconfigurable coincidence counting unit based on an FPGA. To be published (2015).